RESEARCH ARTICLE

WILEY

Determination of groundwater discharge rates and water residence time of groundwater-fed lakes by stable isotopes of water (^{18}O, ^{2}H) and radon (^{222}Rn) mass balances

Eric Petermann[1] 🆔 | John J. Gibson[2,3] | Kay Knöller[4] | Thomas Pannier[1] | Holger Weiß[1] | Michael Schubert[1]

[1] Department of Groundwater Remediation, Helmholtz Centre for Environmental Research – UFZ, Permoserstraße 15, 04318 Leipzig, Germany

[2] InnoTech Alberta, 3-4476 Markham Street, Victoria, BC, Canada

[3] Department of Geography, University of Victoria, P.O. Box 3060 STN CSC, Victoria, BC, Canada

[4] Department of Catchment Hydrology, Helmholtz Centre for Environmental Research – UFZ, Theodor-Lieser-Straße 4, 06120 Halle, Germany

Correspondence
Eric Petermann, Department of Groundwater Remediation, Helmholtz Centre for Environmental Research – UFZ, Permoserstraße 15, 04318 Leipzig, Germany.
Email: eric.petermann@ufz.de

Abstract

Lacustrine groundwater discharge (LGD) and the related water residence time are crucial parameters for quantifying lake matter budgets and assessing its vulnerability to contaminant input. Our approach utilizes the stable isotopes of water (δ^{18}O, δ^{2}H) and the radioisotope radon (^{222}Rn) for determining long-term average and short-term snapshots in LGD. We conducted isotope balances for the 0.5-km^2 Lake Ammelshainer See (Germany) based on measurements of lake isotope inventories and groundwater composition accompanied by good quality and comprehensive long-term meteorological and isotopic data (precipitation) from nearby monitoring stations. The results from the steady-state annual isotope balances that rely on only two sampling campaigns are consistent for both δ^{18}O and δ^{2}H and suggested an overall long-term average LGD rate that was used to infer the water residence time of the lake. These findings were supported by the good agreement of the simulated LGD-driven annual cycles of δ^{18}O and δ^{2}H lake inventories with the observed lake isotope inventories. However, radon mass balances revealed lower values that might be the result of seasonal LGD variability. For obtaining further insights into possible seasonal variability of groundwater–lake interaction, stable water isotope and radon mass balances could be conducted more frequently (e.g., monthly) in order to use the derived groundwater discharge rates as input for time-variant isotope balances.

KEYWORDS

groundwater discharge, groundwater–lake interaction, isotope balance, radon, stable isotopes of water, water balance, water residence time

1 | INTRODUCTION

Lakes provide a wide range of ecosystem services such as a habitat for freshwater species, climate change mitigation, sediment and nutrient retention, and processing as well as hydrological regulation (Schallenberg et al., 2013). Hence, lakes represent valuable aquatic ecosystems, which are exposed to various anthropogenic pressures related to human demands such as recreation, fisheries, or water abstraction. The lakes ecosystem health and the fulfilment of user's demands are highly dependent on its water quality, which is directly linked to the quality of discharging waters and the water residence time within the lake. Groundwater discharge into lakes or lacustrine groundwater discharge (LGD) is often neglected in lake water balances

due to difficulties in its determination. However, several authors have shown that LGD may dominate the water balance both for lakes with (e.g., Kidmose et al., 2013; Rosenberry & Winter, 2009) and without (e.g., Stets, Winter, Rosenberry, & Striegl, 2010; Zhou, Kang, Chen, & Joswiak, 2013) surface water inlets or outlets. Consequently, LGD may also play a crucial role in the lakes geochemical budgets, for example, due to the input of nutrients (Nakayama & Watanabe, 2008) or of sulphate and iron into post-mining lakes ("acid mine drainage"; Knöller et al., 2004; Knöller & Strauch, 2002), both of which represent a serious problem for lake water quality. Another key factor for lake water quality is its residence time. This parameter is a determinant of ecological health because water residence time governs the exposure time to chemical substances introduced into the lake. For instance, longer

water residence times may favour the growth of harmful cyanobacteria (Romo, Soria, Fernandez, Ouahid, & Baron-Sola, 2013).

Several methods for determining LGD exist including watershed-scale studies, lake-water budgets, combined lake-water and chemical budgets, well and flow-net analysis, groundwater flow modelling, tracer studies, thermal methods, seepage meters, and biological indicators (Rosenberry, Lewandowski, Meinikmann, & Nützmann, 2015). Several authors calculated discharge rates from hydraulic gradients between lake and groundwater and hydraulic properties of the aquifer and lake bed sediments (Kishel & Gerla, 2002; Rudnick, Lewandowski, & Nützmann, 2015). A major difficulty of this approach is that the results depend on small differences of hydraulic heads and small-scale variations of the hydraulic conductivity that may fall in the range of measurement uncertainty. Numerical groundwater flow modelling (Wollschläger et al., 2007) requires high-quality a priori information that might not be available in many cases. The only approach for direct measurement of LGD is seepage meters (Rosenberry, LaBaugh, & Hunt, 2008). While providing precise point-scale information, a general drawback of seepage meters is that they may not be spatially representative because LGD is known to be highly heterogeneous in many lakes. Whereas direct measurements are limited to specific areas or lakeshore sections, mapping of geochemical tracers allows obtaining an integrated signal of the entire water body.

Stable isotopes of water (J. J. Gibson, Birks, & Yi, 2016; J. J. Gibson, Birks, Yi, Moncur, & McEachern, 2016; Hofmann, Knöller, & Lessmann, 2008; Knöller et al., 2004; Knöller & Strauch, 2002; Krabbenhoft, Anderson, & Bowser, 1990) and the radioisotope radon (Corbett, Burnett, Cable, & Clark, 1997; Dimova & Burnett, 2011; Schmidt, Stringer, Haferkorn, & Schubert, 2008) or a combination of both (Arnoux, Barbecot, et al., 2017; Arnoux, Gibert-Brunet, et al., 2017; Schmidt, Gibson, Santos, Schubert, & Tattrie, 2009) are well-established in groundwater–lake interaction studies. For instance, Luo, Jiao, Wang, and Liu (2016) and Dimova and Burnett (2011) reported on significant temporal variation of LGD on a multi-day time-scale based on radon for a Chinese desert lakes and small lakes in central Florida (United States), respectively. Kluge et al. (2012) and Dimova, Burnett, Chanton, and Corbett (2013) demonstrated LGD variability also on a seasonal timescale. Arnoux, Barbecot, et al. (2017) applied both radon and stable isotopes to determine intra-annual LGD variability into a small glacial lake in Quebec (Canada).

Stable isotope-based LGD estimates are highly dependent on the relative air humidity and the isotopic composition of the atmospheric vapour and the evaporate (Arnoux, Barbecot, et al., 2017; Hofmann et al., 2008; Knöller & Strauch, 2002). Radon-based estimates depend mainly on the radon concentration of the groundwater endmember and on the quantification of atmospheric radon losses and diffusive radon inputs (Arnoux, Barbecot, et al., 2017; Dimova & Burnett, 2011). All of these parameters are prone to error. However, simultaneous use of stable water isotopes and radon decreases the uncertainty of LGD rate estimates and of the corresponding water residence time. We want to emphasize that both methods indicate LGD rates at different timescales. Although the mean stable water isotope inventory reflects the average conditions during the entire water residence time (usually months to several years), radon-based approaches rather reflect a

snapshot of LGD rate representing a period of maximum of 20 days (five ^{222}Rn half-lives, $t_{1/2} = 3.8$ days).

In the presented study, we determined LGD and derived water residence times for the 0.5-km^2 groundwater-fed Lake Ammelshainer See (Germany) based on field observations of the stable water isotopes (^{18}O, ^{2}H) and the radionuclide radon (^{222}Rn). Both approaches utilize gradients of these tracers between groundwater and lake water and rely on additional climatic and isotopic information. This study demonstrates the potential of combined $\delta^{18}O/\delta^2H$ and Rn mass balances to study LGD at different timescales. The key issue of this study is to demonstrate the power of stable isotope techniques for estimating the long-term mean LGD rate and the corresponding water residence time of groundwater-fed lakes based on a relatively small amount of field data (lake isotope inventories and groundwater isotope composition) accompanied by good quality and comprehensive long-term meteorological and isotopic data (precipitation) from nearby monitoring stations. This approach requires the determination of the mean stable water isotope inventory of the lake and the estimation of the stable isotope signature of the evaporate using the stable isotope signatures of lake, groundwater, and precipitation. The combination of the estimated LGD rate with the meteorological and isotopic data allows the simulation of the annual cycle of the lakes stable water isotope inventory that can subsequently be compared with the observations of the lake inventory at specific dates. The additional application of a radon mass balance (RMB) illustrates the potential for determining LGD rates at temporal snapshots that supports the study of temporal LGD variability.

2 | MATERIAL AND METHODS

2.1 | Theoretical background

2.1.1 | Water balance of groundwater-fed lakes

Groundwater-fed lakes (or "through-flow" lakes) gain water, aside from direct precipitation on the lake, by continuous discharge of groundwater into the lake, which is balanced by a combination of evaporation and water exfiltration, that is, outflow into the aquifer (J. Gibson, Prepas, & McEachern, 2002). In absence of noteworthy surficial inflows and outflows, the hydrological balance can be written as

$$\frac{\partial V}{\partial t} = P + G_i - E - G_o, \tag{1}$$

where V is the volume of the lake, t is time, P is precipitation, G_i is LGD, E is evaporation, and G_o is groundwater outflow.

2.1.2 | Water residence time of lakes

We recognized some confusion regarding the definition of residence time in the literature, which inhibits direct comparability of residence time estimates and is, thus, impeding the vulnerability assessment. Some authors use the water discharge rate (J. J. Gibson, Birks, & Yi, 2016; Knöller & Strauch, 2002) or the groundwater outflow rate plus evaporation for residence time calculation; other authors use the water outflow while excluding evaporation (Hofmann et al., 2008). As pointed out by Quinn (1992), evaporation is indeed an outflow term

regarding water molecules, but it does not remove conservative dissolved substances from a lake. Whereas the first approach for calculating the residence time refers to a parcel of water, the latter refers to a conservative substance. In this study, we follow the latter definition because it presents the more conservative approach in terms of vulnerability assessment. The mean residence time of water (τ) can be calculated from Equation 2 assuming a well-mixed lake.

$$\tau = \frac{V}{G_o}. \tag{2}$$

2.1.3 | Stable isotope mass balance

The use of $\delta^{18}O$ and δ^2H for determining LGD, groundwater outflow, and lake water residence time is based on an isotope mass balance. For that purpose, the isotope compositions of all components of the lakes water balance are required with δ_L, δ_P, δ_{Gi}, δ_{Go}, and δ_E being the isotope composition of the lake, the precipitation, the discharging groundwater, the exfiltrating water, and the evaporation, respectively.

The annual isotope mass balance (Equation 3) follows Equation 1 under the assumption of constant lake volume over time.

$$P\delta_p + G_i\delta_{Gi} = E\delta_E + G_o\delta_{Go}. \tag{3}$$

While assuming the isotope mass balance in interannual steady state, seasonal fluctuations of δ_L as a result of temporal variable LGD and groundwater outflow rates and their respective isotope composition are considered (Equation 4). Following Equation 4, the dynamic isotope mass balance for a well-mixed lake can be written as

$$\delta_{L_{t+1}} = \delta_{L_t} + \frac{\left[P_t\delta_{P_t} + G_i\delta_{G_i} - E_t\delta_{E_t} - G_o\delta_{G_o}\right]}{V}. \tag{4}$$

By assuming a quasi-steady state, that is, a constant seasonal cycle, Equation 4 can be rearranged and solved for G_i or G_O. Although δ_L, δ_P, and δ_{Gi} can be directly measured, δ_{Go} is usually assumed to equal δ_L. In contrast, δ_E cannot be easily measured. However, because evaporation is the process that dominates the evolution of isotope composition of a lake, its accurate estimation is crucial for the precision of water balances. δ_E is calculated (Equation 5) using the linear resistance model of Craig and Gordon (1965) that describes δ_E as a function of relative humidity, air temperature, the isotopic compositions of the lakes surface (δ_{Ls}), and the atmospheric moisture (δ_A). The isotopic composition of δ_{Ls} was parameterized semiquantitatively by assuming an annual cycle with maximum isotopic enrichment at the end of the evaporation season in September and minimum enrichment in winter (Data S1). For parameterization, we utilized the observations of lake surface water in June and September assuming roughly linear enrichment rates during July and August. The isotopic signature at the lake surface for the remaining months October to May was estimated loosely based on the observed annual amplitudes for lakes in the investigated region with most negative values during winter (Hofmann et al., 2008; Knöller & Strauch, 2002; Seebach, Dietz, Lessmann, & Knoeller, 2008).

$$\delta_E = \frac{\frac{\delta_{L_s} - \varepsilon^+}{\alpha^+} - h\,\delta_A - \varepsilon_K}{1 - h + 10^{-3}\varepsilon_K}. \tag{5}$$

The variables in Equation 5 are the equilibrium isotopic separation ε^+ (temperature dependent), the equilibrium isotopic fraction factor α^+ (temperature dependent), the kinetic isotopic separation ε_K (humidity dependent), and the relative humidity h [−]. A detailed description of all calculations required for the isotope mass balance can be found elsewhere (e.g., J. J. Gibson, Birks, & Yi, 2016).

δ_A can either be measured or estimated from δ_P and air temperature. J. J. Gibson, Birks, and Yi (2016) introduced the seasonality factor k [−], which compensates for the effect of seasonality on isotopic fractionation during the evaporation process. This compensation is required because δ_A is usually not in equilibrium with δ_P throughout the year in seasonal climates. The seasonality factor k ranges from 0.5 for highly seasonal climates to 1 for nonseasonal climates and is estimated by dual analysis of δ^2H and $\delta^{18}O$. For that purpose, the mean annual evaporation flux-weighted δ_A is adjusted (by optimizing k) to fit δ_E (Equation 6) to the local evaporation line (LEL; Gat, 2000).

$$\delta_A = \frac{\delta_P - k\,\varepsilon^+}{1 + 10^{-3}\,k\,\varepsilon^+}. \tag{6}$$

2.1.4 | Radon mass balance

RMBs assume equilibrium over time between radon (^{222}Rn) inputs and Rn losses and are a common approach for determining LGD rates to surface water bodies such as lakes, rivers, or the sea (Burnett & Dulaiova, 2003; Dimova & Burnett, 2011; Gilfedder, Frei, Hofmann, & Cartwright, 2015; Schmidt et al., 2008). After accounting for all radon sources and sinks within the considered system, the residual Rn flux [Bq·m^{-2}·day^{-1}] that is required for mass balancing is attributed to LGD. Finally, for conversion of Rn flux to water discharge [m^3 day^{-1}], the resulting groundwater-borne Rn flux (F_{GWi}) is divided by the Rn concentration of groundwater [Bq m^{-3}]. Our RMB is defined as follows:

$$F_{GW_i}\left[\text{Bq m}^{-2}\text{ day}^{-1}\right] = F_{dec} + F_{atm} - F_{dif} - F_{prod}. \tag{7}$$

Rn decay flux (F_{dec}) solely depends on the Rn inventory of the lake and the Rn decay constant ($\lambda_{Rn} = 2.098 * 10^{-6}\,s^{-1}$). The atmospheric Rn flux (F_{atm}, Equation 8) or Rn evasion [Bq m^{-3}] is driven by the Rn concentration gradient between lake surface water (Rn_s) and air (Rn_{air}) and the wind speed [m s^{-1}], which acts as a proxy for the turbulence in the surface layer. In Equation 8, the term a [−] refers to the Rn partitioning coefficient between water and air (Schubert, Paschke, Lieberman, & Burnett, 2012), and K [m day^{-1}] is the Rn transfer velocity (MacIntyre, Wanninkhof, & Chanton, 1995).

$$F_{atm_t}\left[\text{Bq m}^{-2}\text{ day}^{-1}\right] = (Rn_s - a * Rn_{air}) * K. \tag{8}$$

As a consequence of wind speed variability, F_{atm_t} [Bq·m^{-2}·day^{-1}] is temporally highly dynamic. Moreover, the effect of Rn degassing on the Rn inventory of a water body is a result of the wind speed intensity not only during sampling but also during the days prior to sampling. This is the result of the systems "memory effect" regarding Rn degassing. If Rn is removed from a water body after an intense storm event, several days with "normal" wind conditions are required to build up the pre-storm inventory. To account for this memory effect, we

considered the wind speed not only on the day of measurement but also during the days prior to measurement. Therefore, we calculated F_{atm} (Equations 8 and 9) for a period of 10 days prior to sampling by introducing a weighting factor w_t that reflects the effect of an evasion event prior to sampling on the observed Rn inventory.

$$w_t \; [-] = e^{-\lambda_{Rn}*t}. \tag{9}$$

$$F_{atm} \left[Bq\, m^{-2}\, day^{-1} \right] = \frac{\sum_{t=0}^{t_{max}} [w_t * F_{atm\,t}]}{\sum_{t=0}^{t_{max}} w_t}. \tag{10}$$

The weighting factor was parameterized utilizing the Rn decay rate, which is expected to be the primary driver of the systems memory effect. Because MacIntyre et al. (1995) stated a coefficient of determination of 0.66 for their gas flux model, we derived an uncertainty of 34% for F_{atm} calculations.

The diffusive Rn flux (F_{dif}, Equation 11) is governed by the Rn concentration gradient between lake bottom water (Rn_L) and bottom sediment pore water (Rn_{PW}). F_{dif} was calculated from a depth-independent model introduced by Martens, Kipphut, and Klump (1980) where n [–] is porosity and D [$m^2\, s^{-1}$] is the diffusion coefficient of Rn in water.

$$F_{dif} \left[Bq\, m^{-2}\, day^{-1} \right] = \sqrt{n*D*\lambda_{Rn}}*(Rn_{PW}-Rn_L)*86,400\, s. \tag{11}$$

After solving the RMB, GW_i [m day^{-1}] is derived by dividing F_{GWi} [Bq·m^{-2}·day^{-1}] by the representative Rn concentration in groundwater (radon endmember) [Bq m^{-3}].

2.2 | Study site

Lake Ammelshainer See (51.296692°N, 12.608284°E) was chosen as a study site because of the absence of any surface water inflow or outflow. Due to its proximity to Leipzig (Saxony, Germany; Figure 1a) where continuous monitoring of stable isotope composition in precipitation is conducted, these data can be assumed as representative for the precipitation falling on the lake. Therefore, additional measurements of stable isotopes in precipitation are not required.

Lake Ammelshainer See is an artificial lake (former gravel pit) with an area of 0.54 km^2 that is located 20 km east of Leipzig. The lake is situated in a lowland landscape characterized by Tertiary and Quaternary sand and gravel sediments. Lake Ammelshainer See has a mean depth of 12 m and maximum depth of 28 m resulting in a volume of 6.7 * 10^6 m^3. The regional groundwater flow direction is not uniform in the vicinity of the lake according to groundwater contour analysis (Figure 1b). LGD is expected at the northern and eastern shore. Schmidt et al. (2008) described the lake as dimictic with a well-mixed water body in spring and autumn and thermal stratification during summer and winter. Groundwater wells in a 5-km radius around Lake Ammelshainer See (Saxonian State Office for the Environment, Agriculture and Geology, 2016) reveal a typical seasonal cycle of groundwater level fluctuations with lowest groundwater levels between September and November and highest groundwater levels from March to April with an average annual amplitude of ~40 cm.

The lake is hydraulically well connected to a phreatic aquifer with a thickness of 20 m. The mean annual air temperature is 10.0 ± 0.7 °C (reference period 2000–2015), annual precipitation is 617 ± 98 mm (reference period 2000–2015), and annual potential evaporation is 682 ± 35 mm (reference period 2001–2010) with ± indicating the interannual variability (one standard deviation).
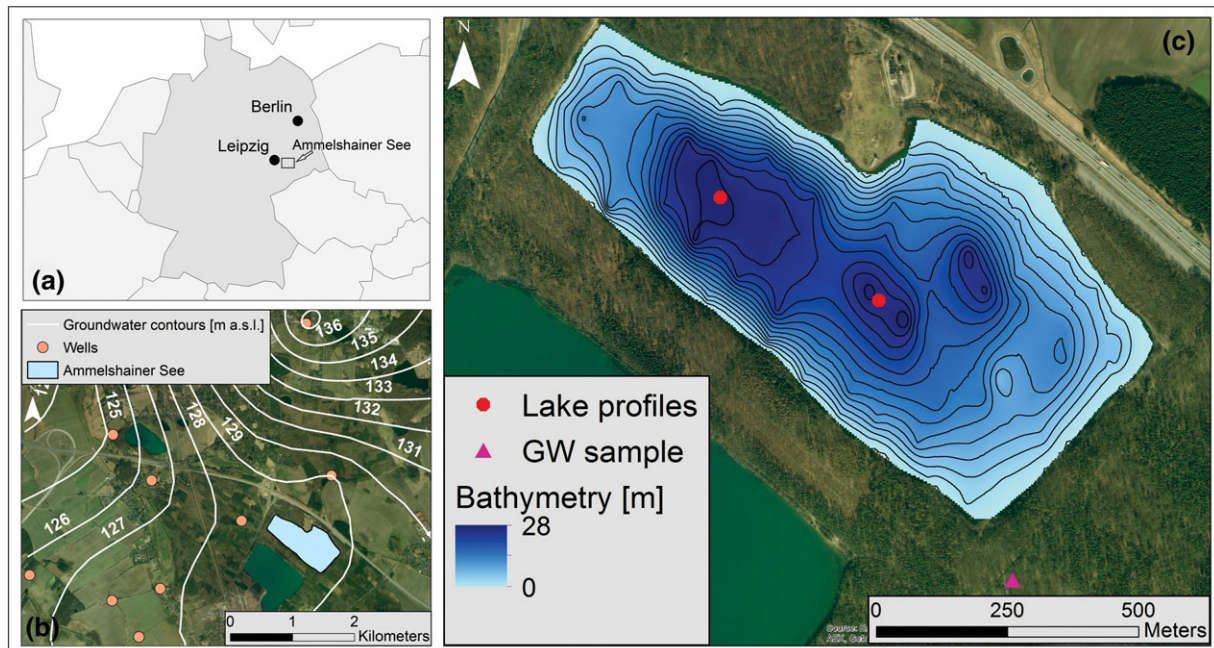

FIGURE 1 Study site Lake Ammelshainer See. (a) Location of Lake Ammelshainer See in Germany. (b) Groundwater contours inferred from groundwater monitoring data from 24 wells (Saxonian State Office for the Environment, Agriculture and Geology, 2016). (c) Bathymetry of Lake Ammelshainer See inferred from echo sounding. Further, locations of lake water profiles and the sampled groundwater well are shown

2.3 | Sampling design

Sampling campaigns were conducted on June 3, 2015, June 9, 2016, and September 22, 2016. In June 2015, the Rn concentration distribution at the lake surface was mapped, Rn depth profiles were measured, and stable isotope sampling at the lake surface was conducted at multiple locations. In June 2016 and September 2016, sampling focused on two depth profiles of stable water isotopes. In September 2016, two Rn depth profiles were additionally measured at the same locations. Groundwater was sampled from a well tapping the uppermost unconfined aquifer that is located less than 100 m south of the lake in the up-gradient area. The well is filtered from a depth of 7.8 m; the groundwater level was 3.4 m below the surface during sampling.

2.4 | Analytical techniques

2.4.1 | Stable water isotopes

Samples for the analysis of oxygen and hydrogen in water were filtered through a 0.2-μm syringe filter and filled into gas-tight 1.5-ml glass vials. Stable isotope analyses of ^{18}O and ^2H were carried out using laser cavity ring-down spectroscopy (Picarro L2120-i, Santa Clara, USA) without further treatment of the water samples. The isotope ratios of $^{18}O/^{16}O$ and $^2H/^1H$ are conventionally expressed in delta notations of their relative abundances as deviations in per mil (‰) from the Vienna Standard Mean Ocean Water (VSMOW). Samples were normalized to the VSMOW scale using replicate analysis of internal standards calibrated to VSMOW and Standard Light Antarctic Precipitation (SLAP) certified reference materials. The analytical uncertainty of the $\delta^{18}O$ measurement is ±0.1‰, for hydrogen isotope analyses, an analytical error of ±0.8‰ has to be considered.

2.4.2 | Radon

The Rn concentration of lake water was measured employing two on-site mobile Rn-in-air monitors AlphaGuard PQ 2000 (Saphymo) that were operated in parallel following Schubert, Buerkin, Peña, Lopez, and Balcázar (2006), whereas the Rn concentration of groundwater samples was measured using the mobile Rn-in-air monitor RAD 7 (Durridge Company). The Rn mapping on lake was executed by boat cruises. For both, lake water and groundwater, Rn was measured from a permanent water pump stream (water flow rate of 2 L min^{-1}) that was connected to a Rn extraction unit (MiniModule® by Membrana GmbH, Germany) where Rn equilibrates between water pump stream and a closed air loop as a consequence of temperature-dependent Rn partitioning between water and air (Schubert et al., 2012). Each sample of the depth profile was measured for 30–40 min after water–air equilibration to obtain at least three replicate measurements at each depth (counting cycle 10 min). Groundwater samples were measured for 30–40 min (counting cycle 5 min) after water–air equilibration to obtain at least six replicate measurements. Equilibration times were ~10 min for the AlphaGuard and ~40 min for the RAD7.

2.5 | Climate, groundwater, and isotope data

Data of air temperature, precipitation, and relative humidity (German Weather Service, 2016) were derived from for nearby stations Leipzig-Holzhausen (10 km west) and Oschatz (35 km east).

Relative humidity, precipitation rate, and air temperature for Lake Ammelshainer See were derived from the arithmetic mean of the monthly means of both stations for the reference period 2000–2015. Monthly averages of relative humidity range from 0.68 (April to July) to 0.85 (November to December), monthly air temperatures range from 0.9 °C (January) to 19.5 °C (July), and precipitation rates range from 31 mm (February and April) to 86 mm (July). Potential evaporation was calculated by the Turc–Wendling method by Saxonian State Office for the Environment, Agriculture and Geology (2016). Data were derived for the period 2001–2010. Equivalently, potential evaporation from Lake Ammelshainer See was calculated as arithmetic mean of stations Leipzig-Holzhausen and Oschatz. Potential evaporation peaks in July (114 mm) and is lowest in December (11 mm).

Stable isotope signatures of water in precipitation are measured continuously at the Helmholtz Centre for Environmental research (UFZ) in Leipzig. Data of monthly means were available for the period from 2012 to 2014. The isotopic composition has a clear seasonal pattern with a range from −11.1‰ (January) to −5.2‰ (June) and from −78.2‰ (January) to −35.1‰ (August) for $\delta^{18}O$ and δ^2H, respectively. The amount-weighted mean annual composition of precipitation for this period was −8.4‰ for $\delta^{18}O$ and −58.7‰ for δ^2H.

3 | RESULTS

3.1 | Water depth profiles

Depth profiles of Rn, $\delta^{18}O$, and δ^2H were measured to determine the isotope inventories of the lake. In addition, temperature was measured, and deuterium excess, as an indicator for evaporation (Gat, 2000), was calculated. Temperature data indicate higher temperatures in the upper part of the lake for June 2016 (17.5 °C) and September 2016 (18.8 °C). Temperatures in deep lake waters were virtually the same in September and June (~8.5 °C) and reflect roughly the mean annual air and groundwater temperature. Rn data were measured in June 2015 and June 2016, that is, at the same seasonal stage of the year. The mean Rn concentration at the lake surface was 31 Bq m^{-3} in both years. Highest Rn concentrations were observed for the deepest samples for both sampling periods. Due to low concentrations and the small number of replicate measurements, analytical uncertainty is comparably high. However, a tendency of higher Rn concentrations with increasing water depth is suggested for both sampling periods. Data on $\delta^{18}O$ and δ^2H reveal similar patterns for both sampling periods: an enrichment of heavier isotopes in the upper layer (down to 4–5 m in June 2016 and to 7–8 m in September 2016) and a relatively constant isotopic composition below that layer. The depth of the isotopic boundary layer correlates well with the thermocline depth. Below a depth of 8 m, isotopic values were found to be −3.7‰ to −3.6‰ for $\delta^{18}O$ and ~−35.5‰ for δ^2H without significant variation with depth. In the upper layer, a clear difference between June and September was recognized for both isotopes. The values were −3.4‰ (June)/−2.8‰ (September) and −34.5‰ (June)/−32.0‰ (September) for $\delta^{18}O$ and δ^2H, respectively. The more pronounced deuterium excess (D excess [‰] = $\delta^2H - 8 * \delta^{18}O$) in the surface layer underpins the causal relationship between isotopic enrichment and evaporation (Gat, 2000).

3.2 | Lake isotope inventory

In order to obtain representative lake isotope inventories, the isotope depth profiles were weighted according to the lake bathymetry. In a first step, a nonlinear asymptotic regression model was fitted to Rn data, and a nonlinear regression model that was adopted from membrane separation techniques was fitted to stable water isotope data (Figure 2). These models provided continuous isotope-depth relationships for all locations. The resulting nonlinear regression models for Rn data (Equation 12) and for stable water isotopes (Equation 13) had the variable z [m], representing the water depth, and the coefficients a, b, c, and d that were fitted to the observed data.

$$Rn = a + b^*e^{c^*z}. \tag{12}$$

$$\delta^{18}O; \delta^2H = \left[a + b^*10^{(c+d^*z)}\right] / \left[1 + 10^{(c+d^*z)}\right]. \tag{13}$$

Subsequently, isotope values were calculated for each water depth of Lake Ammelshainer See. Then, bathymetry was analysed using ArcGIS to obtain the volumetric contribution to lake water of each water depth layer (1-m resolution). For example, the water layer ranging from 0- to 1-m depth comprises 8.2% of the lakes water, the layer from 1- to 2-m depth 7.6%, the layer from 27 to 28 m <0.1%, and so forth. By linking isotope depth profiles with bathymetric analysis, we were able to compute the depth-weighted isotope inventory of the lake. Following this procedure, the lake inventories were calculated with −3.59‰ and −3.23‰ for $\delta^{18}O$ and −35.0‰ and −33.9‰ for δ^2H in June 2016 and September 2016, respectively. Mean Rn concentration was 33.6 Bq m^{-3} in June 2015 and 28.9 Bq m^{-3} in September 2016 (Table 1) that results in lake inventories of 395 and 340 Bq m^{-2} for June 2015 and September 2016, respectively.
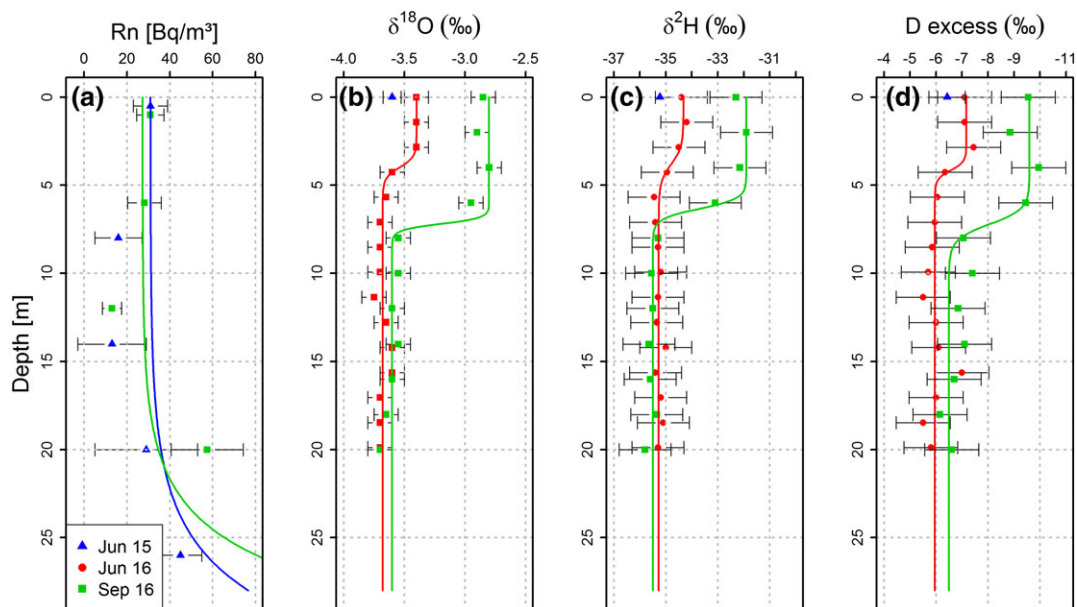
3.3 | Isotope composition in groundwater

The mean composition of $\delta^{18}O$ and δ^2H ($n = 4$) in groundwater was −8.25 ± 0.1‰ and −59.4 ± 1.0‰, respectively. Radon concentration was 18,900 ± 500 Bq m^{-3} ($n = 2$). Variations of both stable water isotopes and Rn were within the analytical uncertainty.

3.4 | $\delta^{18}O$ and δ^2H of the evaporate

The isotopic composition of lake evaporate was estimated by accounting for the $\delta^{18}O$ and δ^2H composition of lake water, groundwater, and precipitation (Figure 3). The groundwater samples plot close to the Local Meteoric Water Line, which indicates that the groundwater is recharged by the local precipitation. In contrast to precipitation and groundwater, lake water samples deviate significantly from the Local Meteoric Water Line as a consequence of isotopic enrichment of lake water due to evaporation. The linear regression model fitted to lake water samples and the sources of lake water (groundwater and amount-weighted annual precipitation) defines the LEL, which is δ^2H = 5.07 (±0.08) * $\delta^{18}O$ − 17.10 (±0.38) ($n = 25, R2 = 0.99$, $p < .0001$). As proposed by J. J. Gibson, Birks, and Yi (2016), the seasonality factor k (2.1.3) was adjusted (Equation 6) aiming at fitting the evaporation flux-weighted annual mean δ_E (Equation 5) to the LEL. In the case of Lake Ammelshainer See, k ranges from 0.73 to 0.78 under consideration of the LEL confidence interval (±1 σ). Accordingly, the evaporation flux-weighted annual mean δ_E ranges from −21.1‰ to −22.8‰ and from −122‰ to −135‰ for $\delta^{18}O$ and δ^2H, respectively.

3.5 | $\delta^{18}O$ and δ^2H mass balance

The input parameters for the isotope mass balance are given in Table 2. The sum of precipitation falling on the lake surface is ~333,000 m^3 a^{-1}, and the sum of evaporation from the lake surface is ~368,000 m^3 a^{-1}.

FIGURE 2 Depth profiles of (a) radon, (b) $\delta^{18}O$, (c) δ^2H, and (d) deuterium excess. Nonlinear regression models (solid lines) were fitted to the observed data that were used for the calculation of isotope inventories. Error bars represent the standard deviation of the two depth profiles (Figure 1c)

TABLE 1 Isotope inventories for sampling campaigns in 2015 and 2016

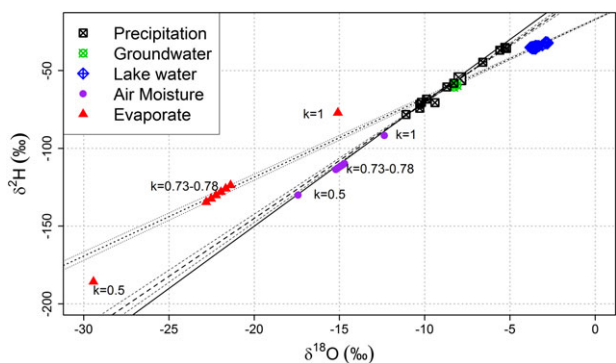| Date	δ^{18}O [‰]	δ^{2}H [‰]	Rn [Bq m^{-2}]
Jun 2015	—[a]	—[a]	395
Jun 2016	−3.59	−35.0	—
Sep 2016	−3.23	−33.9	340

[a]Only measurements at the lake surface.

FIGURE 3 δ^{18}O and δ^{2}H of lake water, precipitation, groundwater, air moisture, and the evaporation for Lake Ammelshainer See. The measured stable isotopes of water in groundwater and lake water as well as the amount-weighted monthly precipitation for 2012–2014 (weather station at UFZ Leipzig) are shown as black squares. The enlarged black square refers to the amount-weighted mean precipitation. The solid line represents the Global Meteoric Water Line, the dashed line the Local Meteoric Water Line, and the dotted line the local evaporation line (LEL). The thinner lines around Local Meteoric Water Line and LEL depict the confidence intervals of the linear regression models (1 σ). The modelled data of the evaporation flux-weighted annual means of the atmospheric moisture (δ$_A$) and the evaporate (δ$_E$) for different seasonality factors (k) that accounts for non-equilibrium fractionation during the evaporation season are shown as purple circles and red triangles, respectively. The possible k values are in the range from 0.73 to 0.78 to force the annual mean evaporate values to lie within the confidence interval of the LEL. δ$_A$ and δ$_E$ for k values of 0.5 (highly seasonal climate) and 1 (nonseasonal climate) are shown for illustrative purposes

The isotopic composition of the lake in June (δ^{18}O$_L$ = −3.59‰ and δ^{2}H$_L$ = −35.0‰) was used as initial value for δ$_L$ and for δ$_{GWout}$ for the dynamic isotope mass balance model. This value was iteratively adjusted to best fit the modelled annual isotope cycle to the observed inventories of δ^{18}O and δ^{2}H in June and September. Accordingly, the optimized value for annual mean δ$_L$ and δ$_{GWout}$ was −3.5‰ and −34.8‰ for δ^{18}O and δ^{2}H, respectively.

Assuming a hydrologic and isotopic interannual steady state, the annual LGD was calculated following Equation 3. The calculated LGD ranged from 1,084,000 to 1,193,000 m^3 a^{-1} for δ^{18}O and 1,027,000 to 1,224,000 m^3 a^{-1} for δ^{2}H. Converted to a mean daily flux, the range of LGD equals 2,800 to 3,350 m^3 day^{-1} for the wider, more conservative error range of δ^{2}H. Accordingly, the mean groundwater outflow rates range from 2,700 to 3,250 m^3 day^{-1}. The determined range of groundwater outflow rates was further used to calculate water residence time in the lake (Equation 3) that ranges from 5.4 to 6.6 a.

For validating the estimated LGD and outflow rates, the annual δ^{18}O and δ^{2}H cycles were simulated with a time-step width of 1 month and compared with the measured isotope inventories in June and September 2016 (Figure 4). Therefore, we used the monthly values presented in Table 1 under assumption of constant LGD over time, which ranges from 3,050 to 3,250 m^3 day^{-1} and from 2,800 to 3,350 m^3 day^{-1} for δ^{18}O and δ^{2}H balance, respectively. Water balances are assumed to be at steady-state on a monthly basis, that is, groundwater outflow rates were calculated to balance LGD, evaporation, and precipitation rates.

The simulated annual cycle is characterized by the most negative isotope values at the end of the non-evaporation season in March and the most positive isotope values at the end of the evaporation season in September. This behaviour is a consequence of the cumulative character of the lakes isotope inventory (Equation 4), that is, during the evaporation season, the lakes isotope inventory is successively enriched in heavier isotopes until the monthly isotope balances are becoming negative in October. In contrast to that, the lakes isotope inventory is constantly depleted in heavier isotopes during the non-evaporation season until the monthly isotope mass balances are becoming positive again in April.

For both isotopes, the modelled seasonal ranges (assuming k values of 0.73 to 0.78) fit well with the observed stable water isotope inventories, although modelled and observed data are in better agreement for δ^{18}O than for δ^{2}H. For δ^{18}O, both observations are within the uncertainty range of the model. For δ^{2}H, the model slightly underestimates the isotope inventory for June and slightly overestimates the isotope inventory for September compared with the observed values.

3.6 | Radon mass balance

The Rn decay losses for the measured lake inventories (3.2) were calculated to be 71.6 and 61.6 Bq·m^{-2}·day^{-1} for June 2015 and June 2016, respectively. Evasion rates were calculated based on wind speed data for a 10-day period prior to the sampling campaigns from the closest weather station (Leipzig-Holzhausen). Wind speed data were available in hourly resolution and are characterized by a median of 2.5 m s^{-1} (range from 0.5 to 5.8 m s^{-1}) for June 2015 and a median of 1.5 m s^{-1} for September 2016 (range from 0.3 to 4.0 m s^{-1}). Additional input data for Rn degassing rate calculation are the Rn concentration in surface water, which was 31 Bq m^{-3} for both campaigns, the measured water temperature at the lake surface (18 °C in June 2015; 19 °C in September 2016), salinity of 0.1 and the Rn concentration in air in the vicinity of the lake of 5 Bq m^{-3}, which is based on previous experience (Schmidt et al., 2008). The weighted Rn degassing rates were 14.5 ± 4.9 Bq·m^{-2}·day^{-1} for June 2015 and 8.3 ± 2.8 Bq·m^{-2}·day^{-1} for September 2016 that basically reflects the differences in wind speed during the days prior to both sampling campaigns.

The required parameters for the calculation of Rn input via diffusion are Rn in sediment porewater, Rn in lake bottom water, porosity, and the Rn diffusion coefficient in water. Rn in sediment porewater underlying the lake was assumed to equal the Rn in groundwater concentration (18,900 ± 500 Bq m^{-3}). Rn concentration in lake bottom water was calculated by the nonlinear regression models discussed in Section 3.1 with ~70 Bq m^{-3}. The Rn diffusion coefficient for the observed temperatures in lake bottom water of 8.5 °C for freshwater is ~7.8 * 10^{-10} m^2 s^{-1} (Schubert & Paschke, 2015). Porosity was

TABLE 2 Climate and isotopic data used as input for stable isotope mass balance and resulting LGD and outflow rates. Relative humidity, air temperature, and precipitation refer to the period 2000–2015, and evaporation refers to the period 2001–2010

Month	Rel. humidity [−]	Air temperature [°C]	Precipitation Rate [mm]	$\delta^{18}O$ [‰]	δ^2H [‰]	Evaporation Rate [mm]	$\delta^{18}O$ [‰]	δ^2H [‰]	LGD Rate [m³ day⁻¹]	$\delta^{18}O$ [‰]	δ^2H [‰]	Groundwater outflow Rate [m³ day⁻¹]
Jan	0.84	0.9	47.5	−11.1	−78.2	13.3	−2.4 to −6.0	−35 to −63	2,800 to 3,350	−8.2	−59.4	3,415 to 3,965
Feb	0.81	1.7	30.8	−10.3	−71.7	20.5	−11.1 to −13.9	−81 to −103	2,800 to 3,350	−8.2	−59.4	2,985 to 3,535
Mrc	0.76	5.0	40.6	−10.3	−74.2	41.2	−15.1 to −17.1	−83 to −98	2,800 to 3,350	−8.2	−59.4	2,790 to 3,340
Apr	0.69	10.0	30.8	−8.7	−60.5	72.2	−21.3 to −22.7	−115 to −126	2,800 to 3,350	−8.2	−59.4	2,055 to 2,605
May	0.70	14.2	62.3	−8.3	−58.1	95.0	−21.5 to 22.8	−114 to −124	2,800 to 3,350	−8.2	−59.4	2,210 to 2,760
Jun	0.69	17.3	55.2	−5.2	−35.9	102.9	−27.7 to −29.0	−154 to −164	2,800 to 3,350	−8.2	−59.4	1,940 to 2,490
Jul	0.69	19.4	85.9	−5.6	−36.9	110.9	−25.9 to −27.2	−145 to −155	2,800 to 3,350	−8.2	−59.4	2,350 to 2,900
Aug	0.70	18.9	71.6	−5.3	−35.1	95.6	−26.0 to −27.4	−149 to −160	2,800 to 3,350	−8.2	−59.4	2,365 to 2,920
Sep	0.77	14.5	56.3	−6.6	−44.7	63.2	−21.3 to −23.3	−137 to −152	2,800 to 3,350	−8.2	−59.4	2,675 to 3,225
Oct	0.82	10.0	38.0	−10.2	−70.4	37.9	−4.9 to −7.8	−47 to −68	2,800 to 3,350	−8.2	−59.4	2,805 to 3,355
Nov	0.85	5.7	53.4	−9.4	−70.6	17.8	−6.3 to −10.1	−40 to −69	2,800 to 3,350	−8.2	−59.4	3,440 to 3,990
Dec	0.85	2.1	44.3	−9.9	−68.4	11.8	−6.8 to −10.6	−66 to −95	2,800 to 3,350	−8.2	−59.4	3,385 to 3,935
Sum			617			682						
Mean	0.77	10.0		−8.0	−55.5		−21.1 to −22.8	−122 to −135	2,800 to 3,350	−8.2	−59.4	2,700 to 3,250

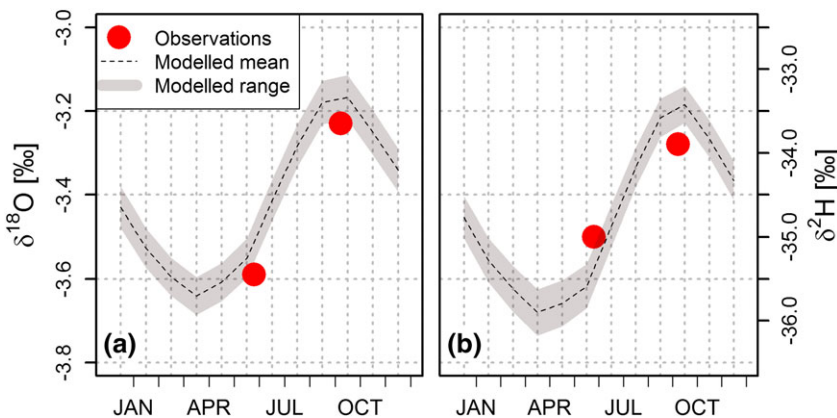*Note.* LGD = lacustrine groundwater discharge.

FIGURE 4 Modelled seasonal cycle of lake isotope inventories of Lake Ammelshainer See. The isotope inventory is driven with calculated signature of the evaporate and groundwater discharge rates and compared with observed isotope inventories. Uncertainty refers to the groundwater discharge range of 2,950 to 3,250 m³ day⁻¹ for $\delta^{18}O$ and 2,800 to 3,350 m³ day⁻¹ for δ^2H that is a result of the uncertainty in determining the isotopic composition of the evaporate (seasonality factor range 0.73–0.78, see Figure 3)

assumed to be 0.35 that is typically for sand and gravel sediments. Finally, the Rn diffusion from the lake bottom sediment porewater into the overlying water column was calculated with 38.9 ± 1.0 Bq·m⁻²·day⁻¹. The required Rn flux to equilibrate the Rn mass balance was 47.4 ± 5.1 Bq·m⁻²·day⁻¹ for June 2015 and 30.9 ± 3.0 Bq·m⁻²·day⁻¹ for September 2016. This residual Rn flux was attributed to LGD. For an Rn concentration in groundwater of 18,900 ± 500 Bq m⁻³, the median LGD velocity averaged over the entire lake area was 2.5 ± 0.3 mm day⁻¹ for June 2015 and 1.6 ± 0.2 mm day⁻¹ for September 2016. Multiplication with the lake surface area of 540,000 m² results in volumetric LGD rates of 1,350 ± 150 m³ day⁻¹ for June 2015 and 900 ± 100 m³ day⁻¹ for September 2016 (Figure 5).

4 | DISCUSSION

The resulting LGD (2,800 to 3,350 m³ day⁻¹) and groundwater outflow rates (2,700 to 3,250 m³ day⁻¹) of Lake Ammelshainer See derived from the steady-state isotopic mass balances are in a similar range for $\delta^{18}O$ and δ^2H (Figure 5). The difference between discharge and outflow is a

consequence of exceedance of evaporation over precipitation with an interannual mean of ~100 m³ day⁻¹ under the assumption of constant lake volume. The LGD rates indicated by $\delta^{18}O$ and δ^2H reflect the long-term (interannual) mean conditions, that is, they represent an integrated value over the entire residence time of water in the lake.

In contrast to that, results from the RMB indicated LGD rates of 1,350 ± 150 and 900 ± 100 m³ day⁻¹ for snapshots in June 2015 and September 2016. These results represent conditions during a few days prior to the sampling campaign basically due to radioactive decay and the evasion intensity of radon (Figure 5). Both processes govern the persistence of a memory effect regarding the Rn concentration in the water body. Consequently, the offset between the stable isotope and the radon-based LGD rates does not necessarily reflect a significant disagreement. Rather, the results from the RMB in June and September may reflect lower LGD rates due to seasonality effects. This hypothesis is supported by the observation of seasonal groundwater level fluctuations with lowest levels measured from late summer to mid-autumn. The groundwater level is the key driver of the hydraulic gradient between groundwater and lake water, which in turn governs LGD rates. However, if stable isotope and Rn-based results are
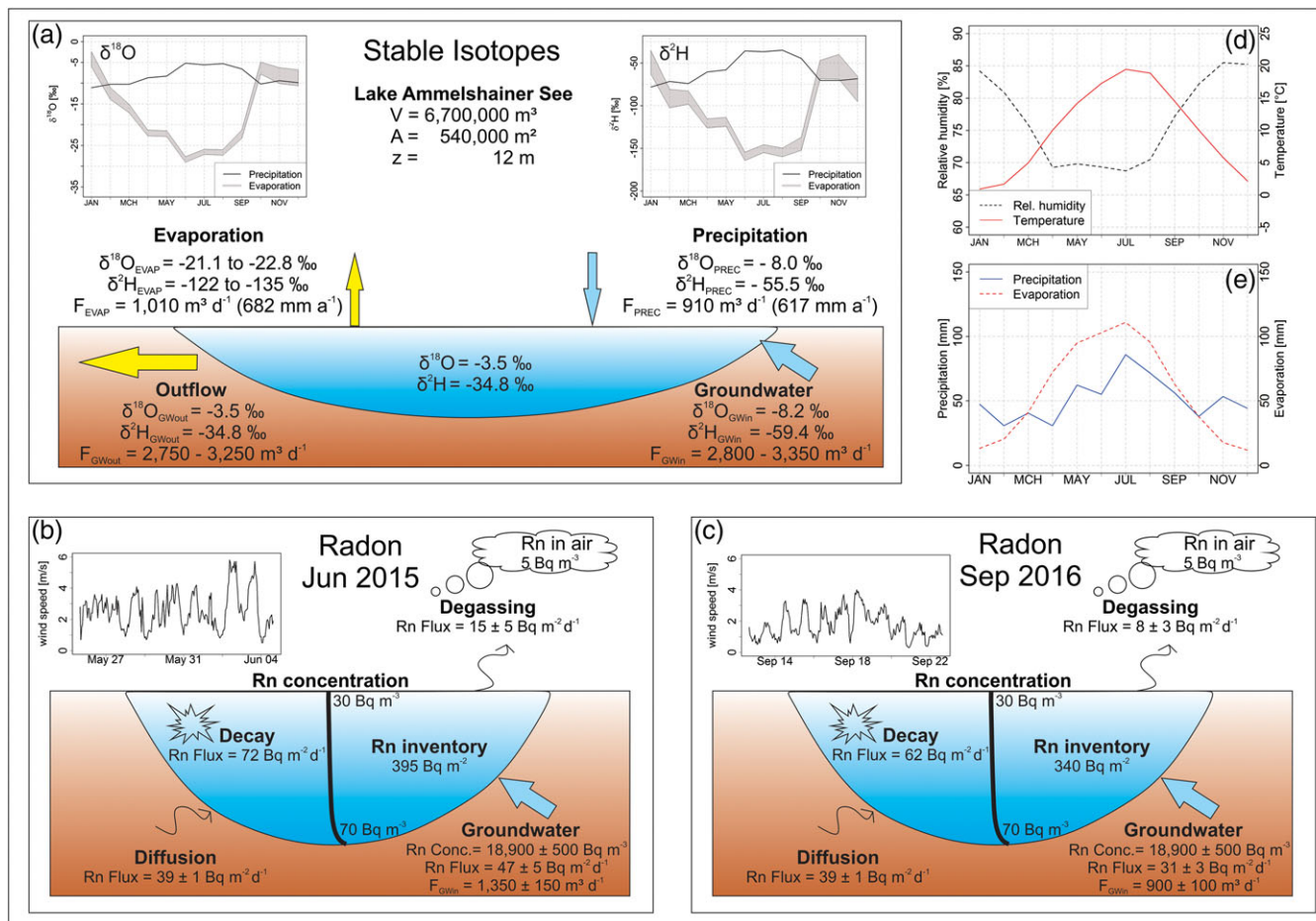
FIGURE 5 Summary of stable water isotopes balances (a) and radon mass balances for June 2015 (b) and September 2016 (c). In (a), monthly isotopic composition of the precipitation and the evaporate are shown for both $\delta^{18}O$ and δ^2H, respectively. Additional climatic data, which are required for stable water isotope mass balances, are air temperature and relative air humidity (d) and precipitation and evaporation rates (e)

both correct, June and September would represent periods with below average LGD rates. This implies that other periods of the year, such as late-winter to late-spring, do likely represent periods with above-average LGD rates to close the stable isotope and water mass balance. Late-winter to early spring typically has higher groundwater levels, which supports this assertion. Still, the hypothesis of temporal varying groundwater discharge rates needs to be validated by additional field campaigns that were beyond the scope of this study. In addition, the radon groundwater endmember relies on one sampled well only that introduces considerable uncertainty. Therefore, the LGD rates inferred from the RMB should be interpreted with care. The accuracy of the radon in groundwater endmember determination needs to be validated in future investigations.

Despite the given uncertainty in LGD estimation, the dominating role of groundwater in the lakes water balance becomes clear by comparing LGD with precipitation (~900 m³ day⁻¹) and evaporation (~1,000 m³ day⁻¹). Thus, LGD rate is a factor of 1 to 3.5 higher than the precipitation rate for Rn- and stable isotope-based estimates.

Our approach for calculating the isotopic composition of the lake evaporate utilizes the slope of the LEL and its uncertainty in a quantitative manner. The observed source water to the lake (i.e., groundwater discharge plus precipitation) is removed either by evaporation, a process that is isotopically fractionating causing enrichment, or by

outflow, which is non-fractionating. Weighted inflow, including contributions from groundwater discharge and precipitation on the lake surface, and mean lake water define a straight line in $\delta^{18}O–\delta^2H$ space (LEL) as a consequence of isotopic fractionation processes, with overall enrichment of lake water determined by conservation of mass. Hofmann et al. (2008), who investigated a lake in a similar climatic setting only 80 km north-east of Lake Ammelshainer See, calculated monthly $\delta^{18}O$ values of the evaporate based on measurements of monthly $\delta^{18}O$ in precipitation and a vapour-precipitation equilibrium approach without considering evaporation seasonality. As a consequence, the isotopic values used in their study showed a much wider spread throughout the year ranging from −30.1‰ (August) to 56.6‰ (November) compared with our study, in which the values ranged from −26.0 to −27.4 (August) up to −2.4 to −6.0 (January; Table 2). The values estimated by Hofmann et al. (2008) are on average slightly more negative during the evaporation season from April to September (~2‰) and dramatically more positive (up to >60‰) during the low-evaporation season compared with our study, although the explanation for the latter observation is unclear. In fact, these very high values calculated by Hofmann et al. (2008) resulted in a relatively heavy mean-weighted $\delta^{18}O$ of the evaporate of −15.4‰ compared with our calculation of −21.1‰ to −22.8‰. Although our use of a seasonality factor for calculating the isotopic composition of the evaporate

remains to be further tested and compared in the study area, it has been applied previously in northern Canada (J. J. Gibson, Birks, & Yi, 2016) and appears to offer a first-approximation approach consistent with the mass balance between inflow terms (groundwater and precipitation), lake water, and evaporate. The simulated annual cycle of $\delta^{18}O$ and δ^2H of lake inventories matches well with the observations in June and September. However, the simulations fit better for $\delta^{18}O$ than for δ^2H, which requires further assessment. Further, a higher number of monitoring wells along the lake shore and depth-differentiated sampling would be favourable to decrease the uncertainty of the stable isotope groundwater endmember that would in turn further increase the validity of the determined LGD rates. The stable isotope composition of groundwater may be spatially heterogeneous and may deviate from the mean-weighted local precipitation for several reasons. For instance, if a considerable share of the catchment area is covered by lakes, evaporation from these lakes could generate an evaporation signal in stable water isotopes of lake water entering the aquifer. Consequently, the groundwater entering the lake of interest may already show an evaporation signal.

A RMB for Lake Ammelshainer See was previously conducted by Schmidt et al. (2008). The authors of this study report similar Rn inventories and Rn fluxes attributed to groundwater. However, the LGD rates that they derived are 23 to 41 times higher than our estimates. This discrepancy is mainly a result of the definition of the Rn groundwater endmember. Schmidt et al. (2008) derived the Rn endmember concentrations from sediment batch experiments with ~300 Bq m^{-3}, whereas we found Rn concentration in groundwater of ~19,000 Bq m^{-3} in a monitoring well close to the lake (as described above) and assumed those as representative for the composition of the discharging groundwater. This tremendous offset cannot be readily explained by spatial or temporal variability. The differences also highlight the inherent sensitivity of the approach to the definition of the endmember concentrations, an issue also raised by Arnoux, Barbecot, et al. (2017) and Arnoux, Gibert-Brunet, et al. (2017). We considered the actual measurement of Rn in groundwater as more representative for the Rn groundwater endmember because the thickness of the lake bottom sediment layer is only a few centimetres in the littoral zone (Schmidt et al., 2008) where the majority of LGD is expected to occur. Under consideration of the groundwater flow velocity of 22–29 cm day^{-1} in the vicinity of the lake given by Schmidt et al. (2008), a groundwater residence time of less than 1 day within these potentially low Rn sediments would not be sufficient to significantly alter the Rn concentration in groundwater. Our assumption regarding endmember definition is further supported by the reasonable agreement of the Rn- and $\delta^{18}O/\delta^2H$-based estimates in this study. However, due to the large sensitivity of the RMB derived water fluxes to the Rn endmember concentration and the fact that Rn concentration in groundwater is known to be highly variable in space, further measurements of Rn in groundwater at different locations (if available and accessible) are suggested to determine its variability (spatially and temporally). These groundwater samples should be located upstream of the lake and close to the lake shoreline to best capture the actual composition of the discharging fluid. The poor data basis regarding Rn in groundwater samples introduces a high uncertainty of the Rn groundwater endmember that limits the reliability of the radon-based LGD estimate. Further, the validity of the radon depth profiles that are required for estimating the radon inventory of the lake needs to be improved in future investigations. For this purpose, the analysis of Rn in the home lab using liquid scintillation counting (Schubert, Kopitz, & Chałupnik, 2014) represents a time efficient alternative for achieving a higher accuracy.

The water residence time of 5.4 to 6.6 years derived from the stable isotope mass balance refers to the residence time of conservative substances (see Section 2.1.2). In addition, we would like to mention that the water residence of a parcel of water itself is 4.2 to 4.8 years, for better comparability with other studies, which was calculated by inclusion of evaporation as a loss term. The offset between residence times depending on how it is defined emphasizes the need for a clear definition of the term "residence time" to allow the regional application of this indicator in vulnerability assessments.

The present approach relies on several assumptions. The reliability and accuracy of the results can be further improved by testing and/or replacing these assumptions with field-based measurements. In our dynamic stable isotope mass balance, assumptions such as constant LGD rate and the constant lake volume may be decisive oversimplifications. In our model, groundwater outflow rates are adjusted to balance seasonally varying evaporation to precipitation ratios to keep the lake volume constant. However, we expect that LGD rates vary over time as a consequence of seasonally varying hydraulic gradients between groundwater and the lake. As a next step, radon and stable isotope mass balances could be conducted at higher temporal resolution (e.g., monthly) for obtaining insight into their seasonal variability. These time-variant LGD rates could be used as input data for time-variant mass balances of $\delta^{18}O$ and δ^2H in combination with lake water level monitoring. This combined approach would help to quantify temporal dynamics and to validate annual averages of LGD rates into lakes. Further, the delineation of the subsurface catchment of the lake determined by a groundwater flow model would be a great advantage, for example, for sampling design and for evaluating the effect of other lakes in the catchment on stable water isotope composition of groundwater. Moreover, in the case of a significant vertical isotopic variability within the aquifer information on depth-dependent discharge rates are of interest for defining the flux-weighted groundwater endmember. Although, in most cases, LGD is focused to the near-shore (e.g., McBride & Pfannkuch, 1975), fine sediment sealing the lake bottom may differentiate this picture.

The presented approach contributes to validation of numerical groundwater flow models for evaluating matter fluxes of, for example, sulphate, acidity, or nutrients into lakes. Further, the introduced procedure can be applied for a comprehensive investigation of LGD and water residence time of groundwater-fed lakes in regions with a dense meteorological and isotopic monitoring network requiring only limited collection of field data.

5 | CONCLUSION

In this study, we present an approach for determining LGD rates into groundwater-fed lakes and for deriving the respective water residence times. The study shows the benefits and limitations of combining

$\delta^{18}O/\delta^2H$ and Rn isotope mass balances for quantification of groundwater connectivity of lakes based on a relatively small amount of field data (lake isotope inventories and groundwater isotope composition) accompanied by good quality and comprehensive long-term meteorological and isotopic data (precipitation) from nearby monitoring stations. The combination of stable isotopes of water and radon offers the opportunity to simultaneously study long-term average conditions and short-term fluctuations of LGD rates. Despite the discussed limitations and uncertainties, the results from both approaches are reasonable and not contradicting. With a greater effort on sampling (e.g., monthly stable isotope and Rn inventories of the lake), further insight into seasonal variability will expectedly be achieved, and uncertainty will be reduced.

ACKNOWLEDGMENTS

ORCID

Eric Petermann http://orcid.org/0000-0002-2305-5026

REFERENCES

Arnoux, M., Barbecot, F., Gibert-Brunet, E., Gibson, J., Rosa, E., Noret, A., & Monvoisin, G. (2017). Geochemical and isotopic mass balances of kettle lakes in southern Quebec (Canada) as tools to document variations in groundwater quantity and quality. *Environmental Earth Sciences*, 76. https://doi.org/10.1007/s12665-017-6410-6

Arnoux, M., Gibert-Brunet, E., Barbecot, F., Guillon, S., Gibson, J., & Noret, A. (2017). Interactions between groundwater and seasonally ice-covered lakes: Using water stable isotopes and radon-222 multi-layer mass balance models. *Hydrological Processes*. https://doi.org/10.1002/hyp.11206

Burnett, W. C., & Dulaiova, H. (2003). Estimating the dynamics of groundwater input into the coastal zone via continuous radon-222 measurements. *Journal of Environmental Radioactivity*, 69, 21–35. https://doi.org/10.1016/S0265-931x(03)00084-5

Corbett, D. R., Burnett, W. C., Cable, P. H., & Clark, S. B. (1997). Radon tracing of groundwater input into Par Pond, Savannah River site. *Journal of Hydrology*, 203, 209–227. https://doi.org/10.1016/S0022-1694(97)00103-0

Craig, H., & Gordon, L. I. (1965). Deuterium and oxygen 18 variations in the ocean and the marine atmosphere. Consiglio nazionale delle richerche, Laboratorio de geologia nucleare.

Dimova, N. T., & Burnett, W. C. (2011). Evaluation of groundwater discharge into small lakes based on the temporal distribution of radon-222. *Limnology and Oceanography*, 56, 486–494. https://doi.org/10.4319/lo.2011.56.2.0486

Dimova, N. T., Burnett, W. C., Chanton, J. P., & Corbett, J. E. (2013). Application of radon-222 to investigate groundwater discharge into small shallow lakes. *Journal of Hydrology*, 486, 112–122. https://doi.org/10.1016/j.jhydrol.2013.01.043

Gat, J. R. (2000). Atmospheric water balance—The isotopic perspective. *Hydrological Processes*, 14, 1357–1369. https://doi.org/10.1002/1099-1085(20000615)14:8%3C1357::AID-HYP986%3E3.0.CO;2-7

German Weather Service (2016). Air temperature, precipitation and relative humidity data.

Gibson, J., Prepas, E., & McEachern, P. (2002). Quantitative comparison of lake throughflow, residency, and catchment runoff using stable isotopes: Modelling and results from a regional survey of Boreal lakes. *Journal of Hydrology*, 262, 128–144.

Gibson, J. J., Birks, S. J., & Yi, Y. (2016). Stable isotope mass balance of lakes: A contemporary perspective. *Quaternary Science Reviews*, 131, 316–328. https://doi.org/10.1016/j.quascirev.2015.04.013

Gibson, J. J., Birks, S. J., Yi, Y., Moncur, M. C., & McEachern, P. M. (2016). Stable isotope mass balance of fifty lakes in central Alberta: Assessing the role of water balance parameters in determining trophic status and lake level. *Journal of Hydrology: Regional Studies*, 6, 13–25. https://doi.org/10.1016/j.ejrh.2016.01.034

Gilfedder, B. S., Frei, S., Hofmann, H., & Cartwright, I. (2015). Groundwater discharge to wetlands driven by storm and flood events: Quantification using continuous radon-222 and electrical conductivity measurements and dynamic mass-balance modelling. *Geochimica et Cosmochimica Acta*, 165, 161–177. https://doi.org/10.1016/j.gca.2015.05.037

Hofmann, H., Knöller, K., & Lessmann, D. (2008). Mining lakes as groundwater-dominated hydrological systems: Assessment of the water balance of Mining Lake Plessa 117 (Lusatia, Germany) using stable isotopes. *Hydrological Processes*, 22, 4620–4627. https://doi.org/10.1002/hyp.7071

Kidmose, J., Nilsson, B., Engesgaard, P., Frandsen, M., Karan, S., Landkildehus, F., ... Jeppesen, E. (2013). Focused groundwater discharge of phosphorus to a eutrophic seepage lake (Lake Væng, Denmark): Implications for lake ecological state and restoration. *Hydrogeology Journal*, 21, 1787–1802. https://doi.org/10.1007/s10040-013-1043-7

Kishel, H. F., & Gerla, P. J. (2002). Characteristics of preferential flow and groundwater discharge to Shingobee Lake, Minnesota, USA. *Hydrological Processes*, 16, 1921–1934. https://doi.org/10.1002/hyp.363

Kluge, T., von Rohden, C., Sonntag, P., Lorenz, S., Wieser, M., Aeschbach-Hertig, W., & Ilmberger, J. (2012). Localising and quantifying groundwater inflow into lakes using high-precision 222Rn profiles. *Journal of Hydrology*, 450-451, 70–81. https://doi.org/10.1016/j.jhydrol.2012.05.026

Knöller, K., Fauville, A., Mayer, B., Strauch, G., Friese, K., & Veizer, J. (2004). Sulfur cycling in an acid mining lake and its vicinity in Lusatia, Germany. *Chemical Geology*, 204, 303–323. https://doi.org/10.1016/j.chemgeo.2003.11.009

Knöller, K., & Strauch, G. (2002). The application of stable isotopes for assessing the hydrological, sulfur, and iron balances of acidic mining lake ML 111 (Lusatia, Germany) as a basis for biotechnological remediation. *Water, Air, & Soil Pollution: Focus*, 2, 3–14. https://doi.org/10.1023/a:1019939309659

Krabbenhoft, D. P., Anderson, M. P., & Bowser, C. J. (1990). Estimating groundwater exchange with lakes: 2. Calibration of a three-dimensional, solute transport model to a stable isotope plume. *Water Resources Research*, 26, 2455–2462.

Luo, X., Jiao, J. J., Wang, X.-S., & Liu, K. (2016). Temporal 222 Rn distributions to reveal groundwater discharge into desert lakes: Implication of water balance in the Badain Jaran Desert, China. *Journal of Hydrology*, 534, 87–103. https://doi.org/10.1016/j.jhydrol.2015.12.051

MacIntyre, S., Wanninkhof, R., & Chanton, J. (1995). Trace gas exchange across the air-water interface in freshwater and coastal marine environments. In *Biogenic trace gases: Measuring emissions from soil and water* (Vol. 5297). Wiley-Blackwell.

Martens, C. S., Kipphut, G. W., & Klump, J. V. (1980). Sediment-water chemical exchange in the coastal zone traced by in situ radon-222 flux measurements. *Science*, 208, 285–288. https://doi.org/10.1126/science.208.4441.285

McBride, M., & Pfannkuch, H. (1975). The distribution of seepage within lakebeds. *Journal of Research of the U.S. Geological Survey*, 3, 505–512.

Nakayama, T., & Watanabe, M. (2008). Missing role of groundwater in water and nutrient cycles in the shallow eutrophic lake Kasumigaura,

Japan. *Hydrological Processes*, 22, 1150–1172. https://doi.org/10.1002/hyp.6684

Quinn, F. H. (1992). Hydraulic residence times for the Laurentian Great Lakes. *Journal of Great Lakes Research*, 18, 22–28. https://doi.org/10.1016/S0380-1330(92)71271-4

Romo, S., Soria, J., Fernandez, F., Ouahid, Y., & Baron-Sola, A. (2013). Water residence time and the dynamics of toxic cyanobacteria. *Freshwater Biology*, 58, 513–522. https://doi.org/10.1111/j.1365-2427.2012.02734.x

Rosenberry, D. O., LaBaugh, J. W., & Hunt, R. J. (2008). Use of monitoring wells, portable piezometers, and seepage meters to quantify flow between surface water and ground water. Field techniques for estimating water fluxes between surface water and ground water. US Geological Survey Techniques and Methods: 4-D2.

Rosenberry, D. O., Lewandowski, J., Meinikmann, K., & Nützmann, G. (2015). Groundwater—The disregarded component in lake water and nutrient budgets. Part 1: Effects of groundwater on hydrology. *Hydrological Processes*, 29, 2895–2921. https://doi.org/10.1002/hyp.10403

Rosenberry, D. O., & Winter, T. C. (2009). *Hydrologic processes and the water budget: Chapter 2* (pp. 23–68). Berkeley: University of California Press.

Rudnick, S., Lewandowski, J., & Nützmann, G. (2015). Investigating groundwater–lake interactions by hydraulic heads and a water balance. *Ground Water*, 53, 227–237. https://doi.org/10.1111/gwat.12208

Saxonian State Office for the Environment, Agriculture and Geology (2016). Groundwater level monitoring data. In *WebGIS Environmental Information System*. Saxonian State Office for the Environment, Agriculture and Geology.

Schallenberg, M., de Winton, M. D., Verburg, P., Kelly, D. J., Hamill, K. D., & Hamilton, D. P. (2013). *Ecosystem services of lakes. Ecosystem services in New Zealand: Conditions and trends.* (pp. 203–225). Lincoln: Manaaki Whenua Press.

Schmidt, A., Gibson, J. J., Santos, I. R., Schubert, M., & Tattrie, K. (2009). The contribution of groundwater discharge to the overall water budget of Boreal lakes in Alberta/Canada estimated from a radon mass balance. *Hydrology and Earth System Sciences Discussions*, 6, 4989–5018. https://doi.org/10.5194/hessd-6-4989-2009

Schmidt, A., Stringer, C. E., Haferkorn, U., & Schubert, M. (2008). Quantification of groundwater discharge into lakes using radon-222 as naturally occurring tracer. *Environmental Geology*, 56, 855–863. https://doi.org/10.1007/s00254-008-1186-3

Schubert, M., Buerkin, W., Peña, P., Lopez, A. E., & Balcázar, M. (2006). On-site determination of the radon concentration in water samples: Methodical background and results from laboratory studies and a field-scale test. *Radiation Measurements*, 41, 492–497. https://doi.org/10.1016/j.radmeas.2005.10.010

Schubert, M., Kopitz, J., & Chałupnik, S. (2014). Sample volume optimization for radon-in-water detection by liquid scintillation counting. *Journal of Environmental Radioactivity*, 134, 109–113. https://doi.org/10.1016/j.jenvrad.2014.03.005

Schubert, M., & Paschke, A. (2015). Radon, CO2 and CH4 as environmental tracers in groundwater/surface water interaction studies—Comparative theoretical evaluation of the gas specific water/air phase transfer kinetics. *The European Physical Journal Special Topics*, 224, 709–715. https://doi.org/10.1140/epjst/e2015-02401-4

Schubert, M., Paschke, A., Lieberman, E., & Burnett, W. C. (2012). Air-water partitioning of 222Rn and its dependence on water temperature and salinity. *Environmental Science & Technology*, 46, 3905–3911. https://doi.org/10.1021/es204680n

Seebach, A., Dietz, S., Lessmann, D., & Knoeller, K. (2008). Estimation of lake water–groundwater interactions in meromictic mining lakes by modelling isotope signatures of lake water. *Isotopes in Environmental and Health Studies*, 44, 99–110. https://doi.org/10.1080/10256010801887513

Stets, E. G., Winter, T. C., Rosenberry, D. O., & Striegl, R. G. (2010). Quantification of surface water and groundwater flows to open- and closed-basin lakes in a headwaters watershed using a descriptive oxygen stable isotope model. *Water Resources Research*, 46. https://doi.org/10.1029/2009wr007793

Wollschläger, U., Ilmberger, J., Isenbeck-Schröter, M., Kreuzer, A. M., von Rohden, C., Roth, K., & Schäfer, W. (2007). Coupling of groundwater and surface water at Lake Willersinnweiher: Groundwater modeling and tracer studies. *Aquatic Sciences*, 69, 138–152. https://doi.org/10.1007/s00027-006-0825-6

Zhou, S., Kang, S., Chen, F., & Joswiak, D. R. (2013). Water balance observations reveal significant subsurface water seepage from Lake Nam Co, south-central Tibetan Plateau. *Journal of Hydrology*, 491, 89–99. https://doi.org/10.1016/j.jhydrol.2013.03.030

SUPPORTING INFORMATION

Additional Supporting Information may be found online in the supporting information tab for this article.